Journal of Global Positioning Systems (*2022*)

Vol. 18, No. 1: 41-55

DOI: 10.5081/jgps.18.1.41

Journal of Global Positioning Systems
2022
© CPGPS

Comparative analysis of data quality and performance index for BDS-3 constellation

Zhipeng Ding[1,2], Kaifei He[1,2,*], Ming Li[1,2], Yu Wu[1,2], Yue Zhang[1,2] and Jinquan Yang[1,2]

1. College of Oceanography and Space Informatics, China University of Petroleum (East China), Qingdao, China
2. Technology Innovation Center for Maritime Silk Road Marine Resources and Environment Networked Observation, Ministry of Natural Resources, Qingdao, China

* Corresponding author: Kaifei He, kfhe@upc.edu.cn

Abstract: The global BeiDou-3 Navigation Satellite System (BDS-3) was completed in July 2020. In terms of data processing, the final positioning and baseline solving results will be affected by the quality of the raw observation data. Therefore, it is necessary to analyse and evaluate the data quality of the complete BDS-3 constellation and its service performance. Based on all observing satellites and the open signals from MGEX stations that can track BDS-3, improved software is used to analyse the complete BDS-3 constellation and signals. Moreover, the service performance of BDS-3 is evaluated using self-developed software. The geometric configuration of the complete BDS-3 constellation is found to be slightly better than that of GPS. However, the overall multipath error is about 10 cm higher than that of GPS, although the increased choke of the measured maritime data effectively weakens the multipath error. The pseudorange multipath error of each signal runs in the order B1I>B2a>B2b>B3I>B2a+B2b>B1C; other quality indicators exhibit little difference among bands. In terms of service performance, the carrier phase residuals are 0.17-0.48cm. After data convergence, the relative positioning performance fluctuates around 5 cm of the "true value", although the fluctuations in the vertical direction are up to 10 cm.

Key words: complete BDS-3 constellation; data quality; service performance evaluation

1. Introduction

The first BeiDou-3 Navigation Satellite System (BDS-3) modules were officially launched in 2009, and the last satellite of the network was added in 2020. The 30 satellites that constitute BDS-3 include 24 medium-circle earth orbit (MEO) satellites, three geostationary earth orbit (GEO) satellites, and three inclined geosynchronous orbit (IGSO) satellites [1-3]. BDS-3 provides satellite signals at various frequencies, with the two open-service signals of B1I (1561.098 Hz) and B3I (1268.52 Hz) in the B1 and B3 frequency bands, the B1C frequency band centred on 1575.420 MHz (the same as GPS L1 and Galileo E1), and the B2a frequency band centred on 1176.450 Hz (the same as GPS L5, QZSS L5, IRNSS L5, and Galileo E5a). The most recently launched satellite added the B2a+B2b (1191.795 Hz) signal [4-7]. On December 27, 2019, the B2b signal interface document was published, disclosing two B2b (1207.14 Hz) signals, which provide basic navigation services, and the PPP-B2b signal, which provides precision single-point positioning services [8].

As the basis of BDS data processing, the quality of the original data directly affects the final positioning results or baseline solution. Extensive analysis of the BDS data quality has been conducted, including comparisons with other systems. In terms of quality evaluation, Cai *et al.* (2016) analysed the

Editor in charge: Dr. Baocheng Zhang

noise and multipath effect of BDS-2 based on the zero-baseline double difference, and found that the noise of the B1 band has the largest pseudorange multipath error (mean error of 0.36 cm), whereas the noise of the carrier phase in different frequency bands varies from 0.9-1.5 mm [9]. In 2018, several BDS-3 satellites were launched. Yang *et al.* (2019) studied the basic performance of BDS-3, and reported that the post-processing of the orbit can reach centimetre-level accuracy. Additionally, the average satellite clock offset uncertainty of 18 MEO satellites was found to be 1.55 ns, and the mean ranging error of space signals was about 0.474 m. A method to improve the positioning, navigation, and timing services was subsequently developed [10]. In 2019, some BDS-3 satellites added new signals. Dai *et al.* (2019) studied the noise and multipath level of these BDS-3 signals and satellites, and showed that the standard deviation (STD) of the pseudorange noise in the B1I, B3I, B1C, and B2a bands was 7.4, 6.7, 14, and 13 cm, respectively, whereas the STD of the carrier phase noise was 1.84, 1.85, 1.85, and 1.85 cm, respectively. The STD of the pseudorange multipath errors in bands B1I, B3I, B1C, and B2a was 0.34, 0.21, 0.48, and 0.33 m, respectively [11]. In terms of data service performance, the pseudo-single point positioning and precise single-point positioning (PPP) were tested by Mu *et al.* (2020), who showed that BDS-3 has a slightly lower positioning accuracy than GPS and Galileo, but performs better than GLONASS [12]. Zhang *et al.* (2019) combined the BDS-3 measurement data and showed that the ambiguity resolution efficiency of RTK could be improved by incorporating the BDS-3 measurements, where by the success rate increased from 88.5 to 91.4%. The convergence time of the PPP algorithm was shortened from about 1 h to less than 30 min, and the positioning accuracy was significantly enhanced. Both BDS-3 and GPS can provide centimetre-level dynamic positioning accuracy [13]. Different signal frequency bands exhibit different data service performance. Zhu *et al.* (2021) analysed the new B1C and B2a signals of BDS-3, and found that the positioning performance was comparable to that of GPS and Galileo [14].

Most previous research has focused on BDS-2 or subsets of the BDS-3 satellites. Given the limitations of existing software and the scarcity or incompleteness of signal data, the data quality and basic evaluation methods of BDS-3 have not been systematically tested since the completion of the network. Existing studies have only examined a few BDS-3 satellites and certain signal bands; in particular, the data quality of satellites above C37 has rarely been studied. In this paper, based on all the observable MGEX in-orbit satellite data of BDS-3 and the data quality of the associated signals, indicators related to observation data quality and data service performance are studied and compared with GPS. Comparing and evaluating the complete BDS-3 data quality not only provides a systematic summary of the complete global BDS-3 network, but also lays the foundation for studying the application of BDS-3 in the production process.

2. Architecture of BDS-3 and Dataset Description

Since February 2022, more than 500 IGS tracking stations have been in operation around the world. GNSS multi-mode tracking stations provided the GNSS experimental data for the study of BDS-3 data quality and evaluation of the data performance. The data used in the experiment were divided into static and dynamic data. The static data were taken from the MGEX IGS stations, which can receive all BDS-3 signals. The specific station information is listed in Table 1. The selected observation data were from day of year (DOY) 33-42, 2021. To analyse the global data service performance of BDS-3, data were selected from two stations located in China (WUH2 and URUM) and five stations in other countries (POTS, SGOC, SUTM, ULAB, and WIND).

The satellites that participated in the calculations at each station are listed in Table 2. The GNSS data for the shipboard dynamic experiment were collected from the offshore waters of Tangdao Bay, Qingdao, China, near to the China University of Petroleum (East China), on December 16, 2021, over an observation duration of 2 h. A choke coil was installed on the antenna, as shown in Figure 1.

Table 1 Selected IGS station information

Site	Location	latitude /N	longitude /E	Height/m	Receiver	Antenna
POTS	Germany	52.379	13.066	144.4	JAVAD TRE_3	JAVRNGANT_G5T-NONE
SGOC	Sri Lanka	6.892	79.874	-78.5		
SUTM	South Africa	-32.381	20.811	1797.6		
ULAB	Mongolia	47.865	107.052	1575.7		
URUM	Urumqi	43.808	87.601	858.9		
WIND	Namibia	-22.575	170.189	1734.7		
WUH2	Wuhan	30.532	114.357	25.8		

Table 2 BDS-3 satellites used in the calculations

Site	Satellites involved in the solution
POTS	C19-C30 C32-C46 C60
SGOC	
SUTM	
ULAB	
URUM	
WIND	C20 C21 C23-C30 C32 C33 C34 C36 C37 C38 C40-C46 C60
WUH2	C19-C30 C32-C46

Fig. 1 Dynamic station setup

3. BDS-3 Data Quality Evaluation

3.1 Multipath Error

The multipath combination is a geometry-free and ionosphere-free combination formed by a one-frequency code and two-frequency phase measurements. It contains the combined noise and multipath errors of the code and phase measurements. However, because the noise and multipath errors of the phase are somewhat smaller than those of the code, the combination series mainly reflects the code noise and its multipath error. The GNSS dual-frequency multipath error is usually evaluated using a linear combination of the pseudorange and carrier [15]. The specific calculation can be written as:

$$MP_1 = P_1 - \left(1 + \frac{2}{\alpha - 1}\right) L_1 + \frac{2}{\alpha - 1} L_2 = M_1 + \mathrm{C}_1 - \left(1 + \frac{2}{\alpha - 1}\right) m_1 + \frac{2}{\alpha - 1} m_2 \quad (1)$$

$$MP_2 = P_2 - \left(\frac{2\alpha}{\alpha - 1}\right) L_1 + \left(\frac{2\alpha}{\alpha - 1} - 1\right) L_2 = M_2 + \mathrm{C}_2 - \frac{2}{\alpha - 1} m_1 + \left(\frac{2\alpha}{\alpha - 1} - 1\right) m_2 \quad (2)$$

$$\mathrm{C}_1 = -\left(1 + \frac{2}{\alpha - 1}\right) n_1 \lambda_1 + \left(\frac{2}{\alpha - 1}\right) n_2 \lambda_2 \quad (3)$$

$$C_2 = -\left(\frac{2\alpha}{\alpha-1}\right)n_1\lambda_1 + \left(\frac{2\alpha}{\alpha-1}-1\right)n_2\lambda_2 \quad , \quad \alpha = \frac{f_1^2}{f_2^2} \tag{4}$$

where *MP* represents the multipath error, *M* is the pseudorange multipath error, and *m* is the carrier phase multipath error. When there is no cycle skip, *C* is a constant. *MP* is mainly affected by the pseudorange multipath, because the values of m_1 and m_2 are much smaller than M_1 and M_2, which are used to measure the multipath effect. The multipath errors of BDS-3 visual satellites in all frequency bands were analysed, and the results from each observation station were averaged over 10 consecutive days and compared with GPS. The results are shown in Figures 2 and 3.

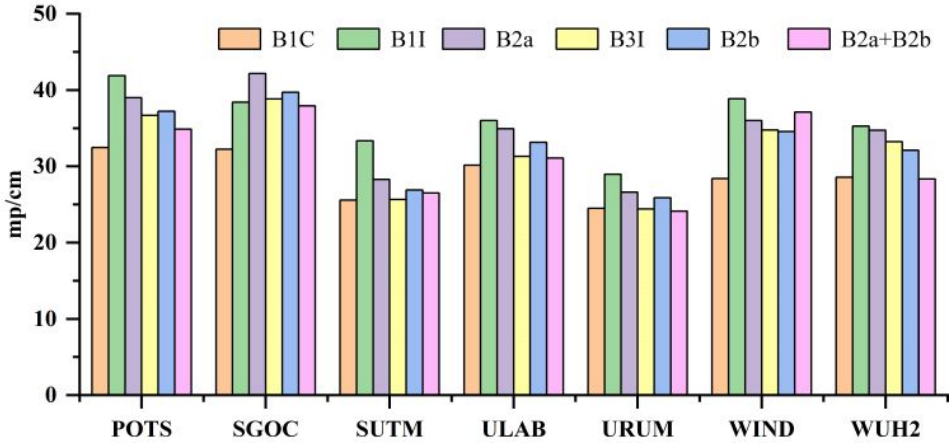

Fig. 2 BDS-3 pseudorange multipath error of station

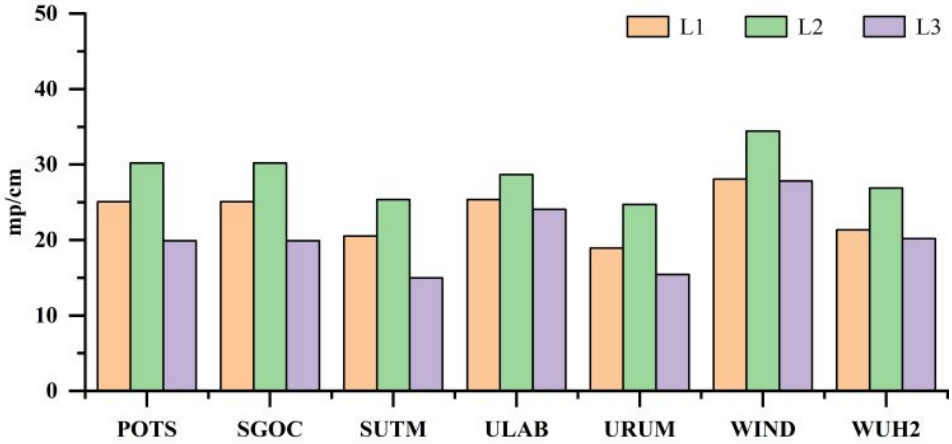

Fig. 3 GPS pseudorange multipath error of station

(1) The multipath errors of each frequency band are slightly different, and the pseudorange multipath errors of each frequency band of BDS-3 run in the order B1I>B2a>B2b>B3I>B2a+B2b>B1C. The largest multipath errors are in bands B1I and B2a, and the maximum value of 42.16 cm appears in band B2a at station SGOC. The smallest multipath error is in band B1C, and the minimum value is 24.10 cm at station URUM.

(2) The multipath error of each frequency band of BDS-3 is worse than that of the GPS data from the same station over the same period. The maximum pseudorange multipath error of GPS is 34.44 cm in band L2 at station WIND, some 7.62 cm smaller than the equivalent value for BDS-3. The minimum GPS pseudorange multipath error of 15.00 cm occurs in band L5 at station URUM. This value is 9.10 cm smaller than the equivalent for BDS-3. Therefore, the multipath error of BDS-3 requires further study.

(3) The pseudorange multipath errors of BDS-3 and GPS exhibit similar trends. For instance, the multipath errors at stations SUTM and URUM are

small, whereas those at stations POTS, SGOC, and WIND are large. These trends are related to the environment and observation conditions of a particular station at that time.

To solve the problem of insufficient research on BDS-3 satellites above C37, four satellites were selected for further analysis: C40 (IGSO), C44 (MEO), C59 (GEO), and G30 (MEO). For these BDS-3 satellites, Figure 4 shows the variation in the multipath effect with respect to elevation angle for each frequency at station WUH2. The multipath errors of the IGSO and MEO satellites exhibit opposite trends with respect to elevation angle. This is mainly because, as the satellite enters or leaves the observation field of view, serious multipath errors and noise occur. The MEO satellite loses significant amounts of data through signal interruption; because the GEO satellite experiences little change in elevation angle, the corresponding multipath error is small and varies gently. Comparing all frequency bands, B1I has the most serious multipath effect among the different orbital types; the GPS satellite and MEO satellite of BDS-3 exhibit the same trend.

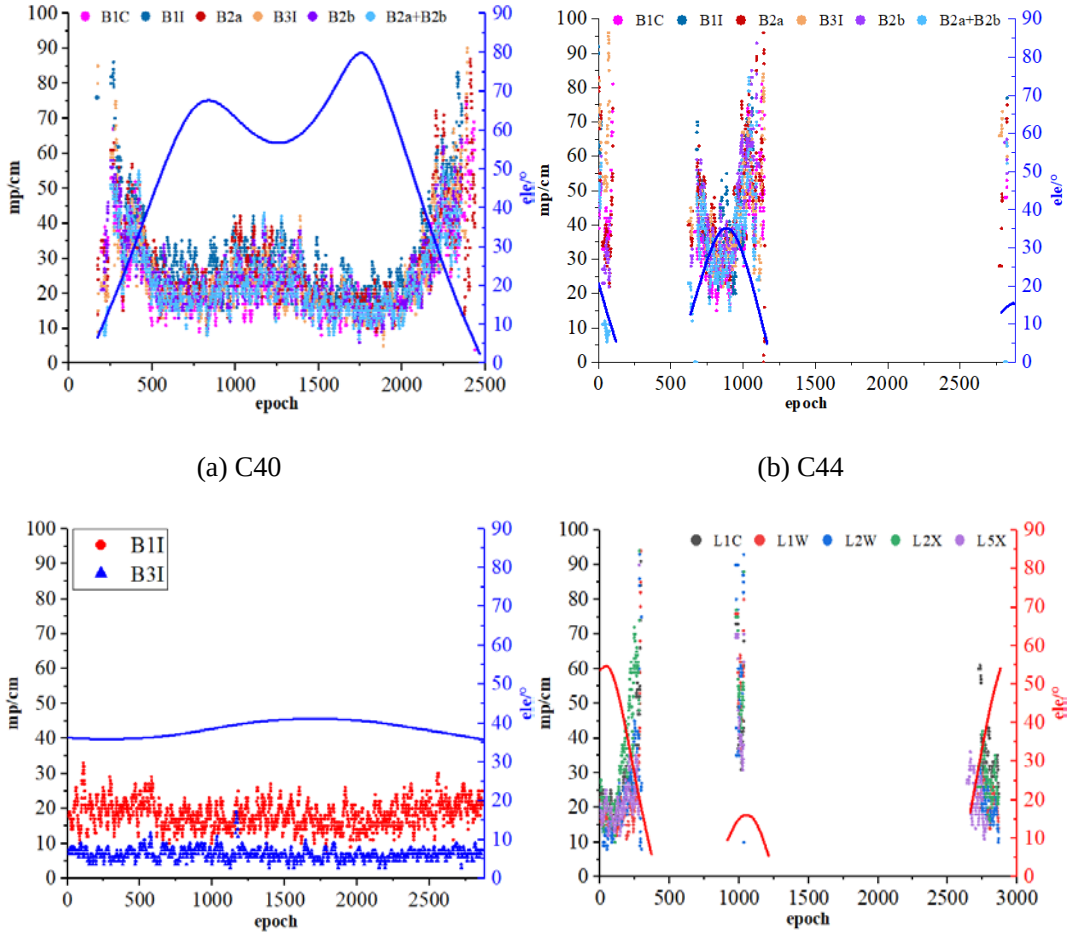

Fig. 4 C40/C44/C59/G30 pseudorange multipath error and elevation angle variation

Next, we analysed the multipath effects of two common frequency bands collected from the sea. Figure 5 shows that, after adding the choke, the multipath error of the two GEO satellites (C59 and C60) is greatly weakened and basically fluctuates around 1 cm. The multipath error of some IGSO and MEO satellites is also weakened, fluctuating around 10 cm. Therefore, the marine dynamic platform effectively reduces the impact of multipath error on BDS-3 service performance through the appropriate placement of choke coils.

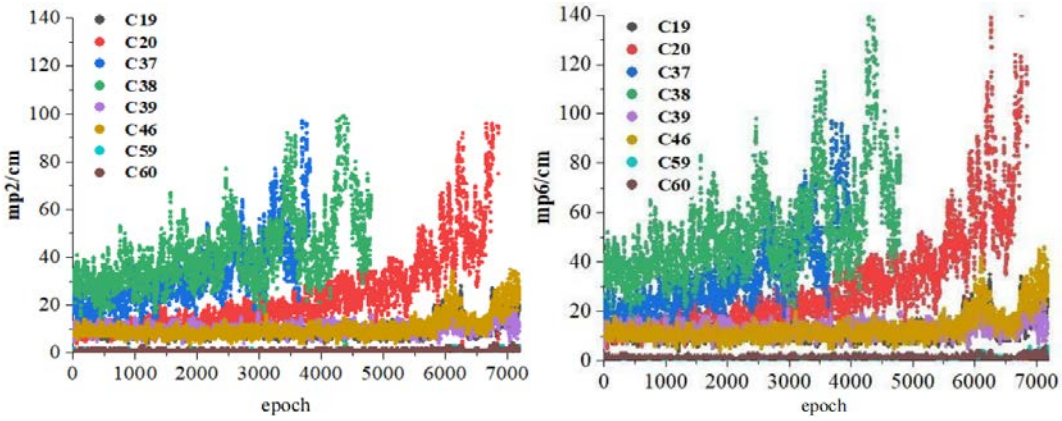

Fig. 5 BDS-3 multipath time series diagram of B1I/B3I

3.2 Signal-to-Noise Ratio

The signal-to-noise ratio (SNR) is the ratio of carrier signal intensity to noise intensity. The SNR level is mainly affected by antenna gain parameters, the state of the correlator in the receiver, and multipath effects. It is one of the indicators reflecting the observation quality of the carrier phase, and is expressed as the ratio of the average power of the signal to the average power of the noise [16]. The SNR of each frequency band at seven stations over 10 consecutive days was averaged and compared with GPS data. The results are shown in Figures 6 and 7.

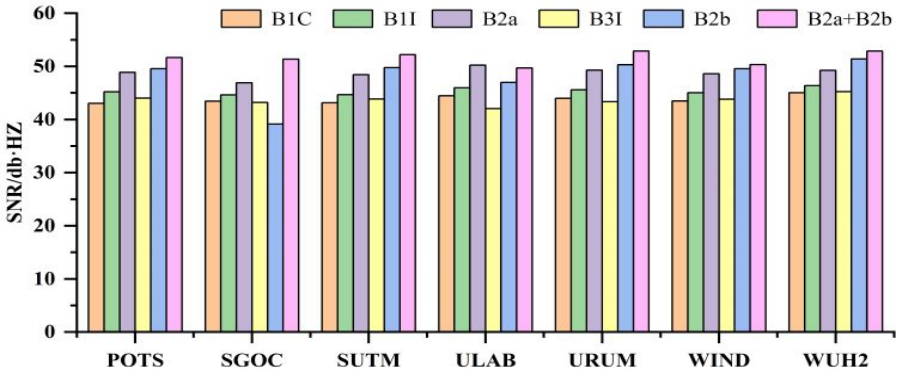

Fig. 6 BDS-3 SNR of stations

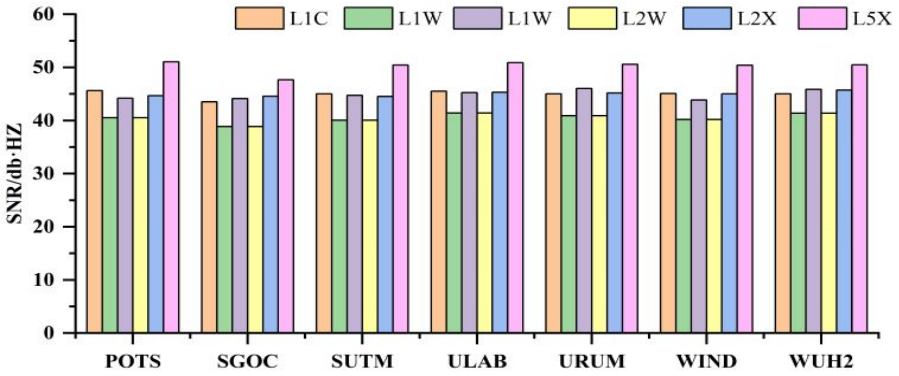

Fig. 7 GPS SNR of stations

(1) Although the SNR of each station in each frequency band is slightly different, the difference between the SNR of BDS-3 in all frequency bands is generally small. However, the SNR of the B2a+B2b frequency band is large. The minimum value of 39.14 dB·Hz in frequency band B2b occurs at station SGOC; by comparison, frequency band B2a+B2b has a maximum value of 52.88 dB·Hz at station WUH2,

a difference of 13.74 dB·Hz.

(2) The SNR of BDS-3 in each band is comparable to that of GPS at the same station. The maximum SNR of GPS is 51.04 dB·Hz in the L5 band at station POTS, which is 1.84 dB·Hz lower than the maximum value of BDS-3. The minimum SNR of GPS is 38.87 dB·Hz in the L1W and L2W bands at station SGOC, some 0.27 dB·Hz larger than the minimum value of BDS-3. The BDS-3 values are basically consistent with the average SNR of each GPS station, and the average SNRs basically fluctuate from 40-50 dB·Hz.

The relationship between SNR and satellite elevation angle is now analysed by examining the C40 (IGSO), C44 (MEO), C59 (GEO), and G30 (MEO) satellites. The results are shown in Figure 8.

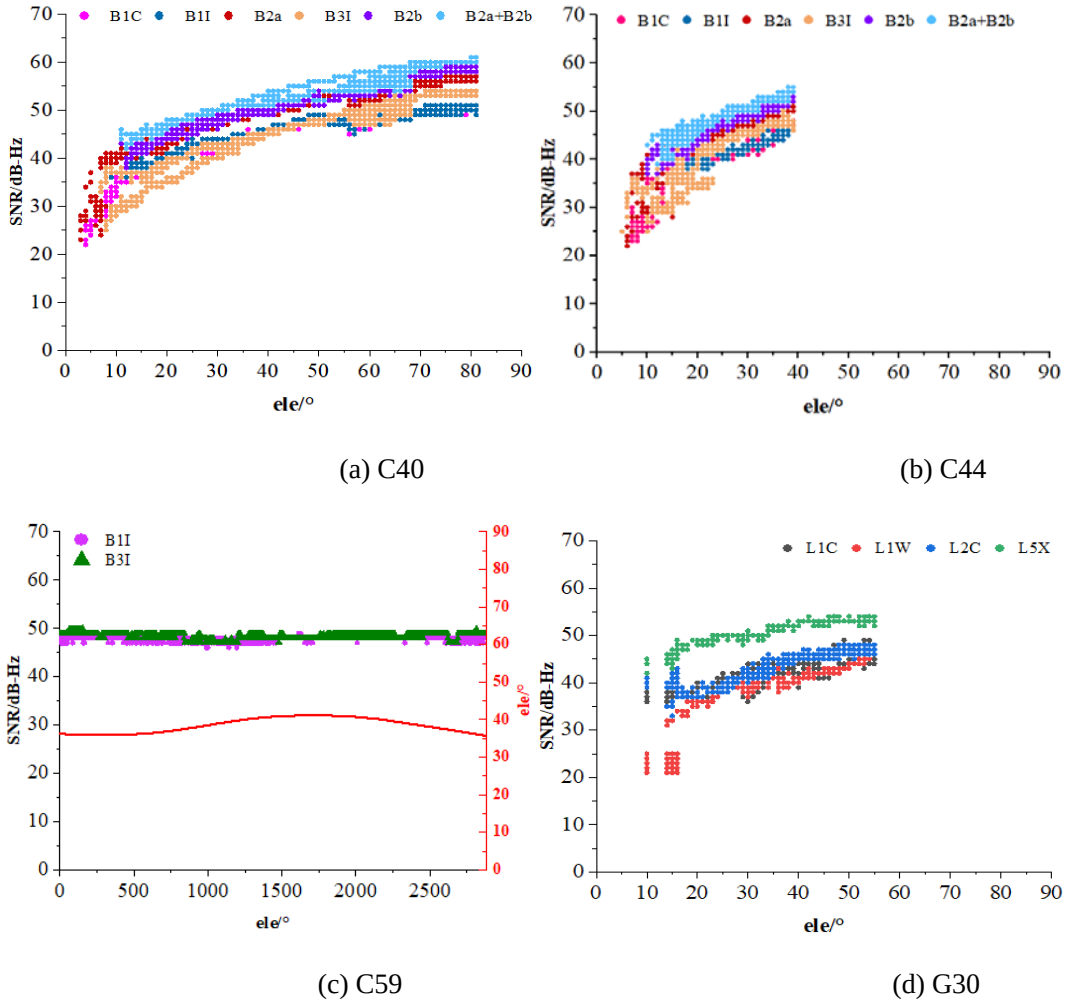

(a) C40

(b) C44

(c) C59

(d) G30

Fig. 8 C40/C44/C59/G30 SNR with respect to elevation angle

Figure 8 shows that the SNR of the IGSO and MEO satellites gradually increases with increasing elevation angle, and varies within the range 22-60 dB·Hz. Because the elevation angle of GEO satellites remains stable, the SNR of the two frequency bands does not change significantly, varying within the range 46-48 dB·Hz. For the IGSO and MEO satellites of BDS-3, the SNR of band B1I is lower than that of the other bands, and the SNR of B2b and B2a+B2b is the highest.

Analysing the SNRs of the measured marine data, Figure 9 indicates that, except for the GEO satellites, the SNR exhibits the opposite trend to that of the multipath effect and contrasts with the observations from static stations. The SNR does not change significantly, basically fluctuating in the range 30-55 dB·Hz.

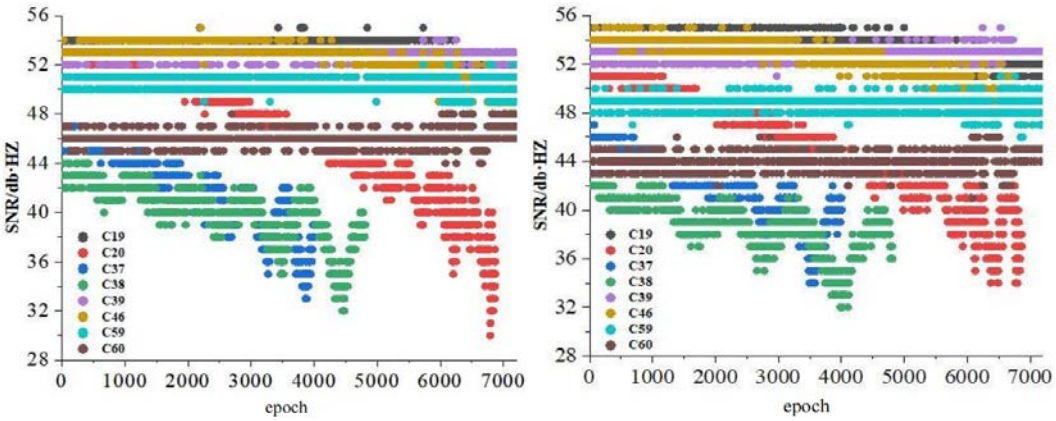

Fig. 9 BDS-3 SNR time series diagram of B1I/B3I

4. BDS-3 Data Service Performance Indicators

4.1 BDS-3 Precision Factor

The service performance of GNSS is related to the spatial geometric configuration of the satellite. In terms of measurement, the dilution of precision (DOP) is often used to describe the basic structure of the spatial geometric distribution of the satellite [17], as shown in the following expressions:

$$Q_X = (B^T PB)^{-1} = \begin{bmatrix} q_{xx} & q_{xy} & q_{xz} & q_{xt} \\ q_{yx} & q_{yy} & q_{yz} & q_{yt} \\ q_{zx} & q_{zy} & q_{zz} & q_{zt} \\ q_{tx} & q_{ty} & q_{tz} & q_{tt} \end{bmatrix} \quad (5)$$

$$GDOP = \sqrt{q_{xx} + q_{yy} + q_{zz} + q_{tt}} \quad (6)$$

$$PDOP = \sqrt{q_{xx} + q_{yy} + q_{zz}} \quad (7)$$

$$HDOP = \sqrt{q_{xx} + q_{yy}} \quad (8)$$

$$VDOP = \sqrt{q_{zz}} \quad (9)$$

The geometric DOP (GDOP) is the distance vector amplification factor between the receiver and the satellite caused by system ranging errors. If the spatial distribution of the satellite is not concentrated in one region and can be evenly distributed in different directions, the positioning accuracy of the satellite is higher than that of the uneven distribution in the same case. The position DOP (PDOP) describes the error caused by the influence of the geometric shape between the satellite and the receiver. A better geometric distribution of satellites in the sky gives a smaller PDOP value and higher positioning accuracy of the satellite system. The horizontal DOP (HDOP) is the square root of the sum of the squares of errors in latitude and longitude, which describes the positioning accuracy in the horizontal direction. The vertical DOP (VDOP) describes the positioning accuracy in the vertical direction. HDOP is consistent with VDOP in that lower values indicate higher positioning accuracy [18].

The mean DOP values of BDS-3 and GPS over 10 consecutive days at all seven stations are shown in Figure 10.

Figure 10(a) shows that, except for stations WIND and SUTM, the PDOP value of BDS-3 is slightly lower or equivalent to that of GPS. The largest difference appears at station WUH2, where the BDS-3 PDOP is 0.46 lower than that of GPS. This indicates that the distribution of BDS-3 in the sky is slightly better than that of GPS satellites. From Figure 10(b), it is apparent that the GDOP of BDS-3 is equivalent to that of GPS, except at stations ULAB and WUH2. At these stations, BDS-3 has a smaller GDOP than GPS, and the maximum difference reaches 0.78 at ULAB. The horizontal and vertical accuracy factors exhibit similar variation trends as GDOP and PDOP. BDS-3 has slightly higher values than GPS at three stations, and lower values than GPS at the other four stations. The largest differences occur at station WUH2, where the HDOP and VDOP values of BDS-3 are 0.28 and 0.34 lower than those of GPS, respectively. Thus, in general, the error

magnification of BDS-3 is smaller than that of GPS.

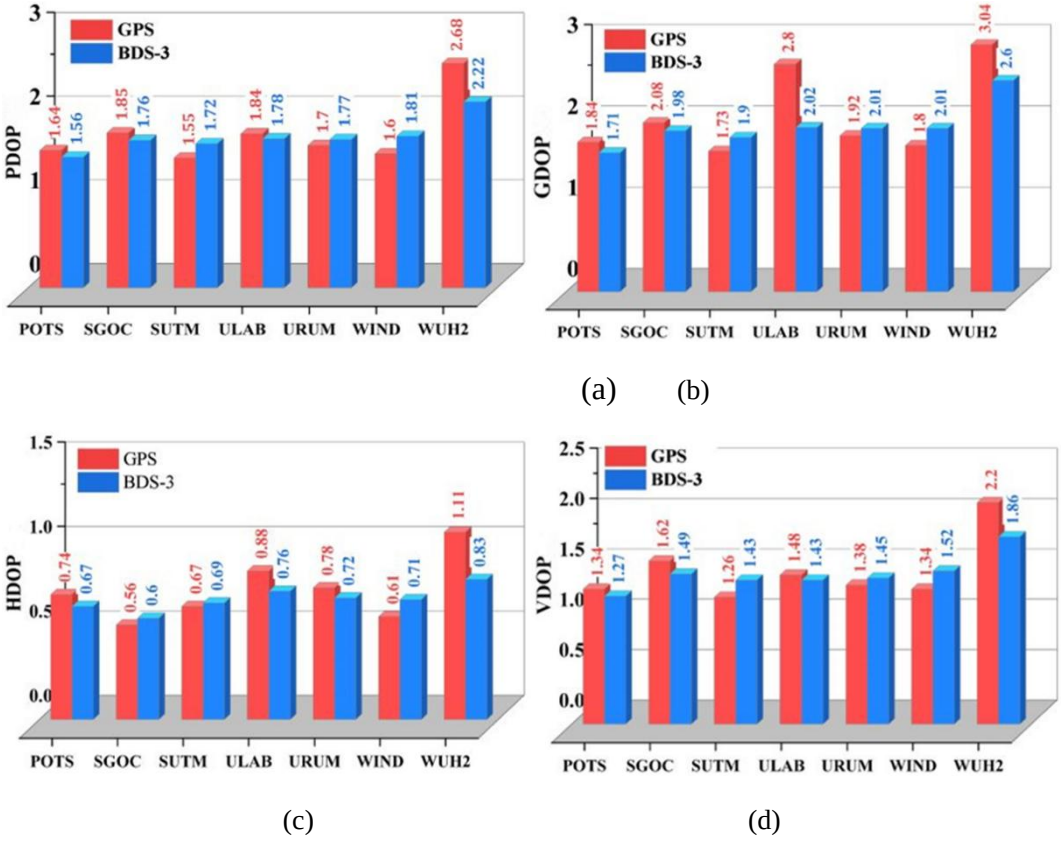

Fig. 10 BDS-3/GPS precision factor at each station

The horizontal precision factor of BDS-3 and GPS is smaller than the vertical precision factor, indicating that the horizontal accuracy is greater than the vertical accuracy. The maximum HDOP and VDOP of BDS-3 at station WUH2 are 1.11 and 2.20, respectively.

4.2 Three-Difference Residual of Carrier Phase

The precision of carrier phase observations can often reach the millimetre level. These observations can be combined with pseudorange observations to detect cycle slip. Because the observation values do not vary much over short periods of time, the precision of carrier phase observations can be expressed using the three-difference method. The adjacent epochs between each frequency band are changed three times to obtain L^3, which is used to evaluate the accuracy of the carrier phase observations. The evaluation method can be written as:

$$\begin{aligned} \Delta L_i^1 &= L_i - L_{i-1} \\ \Delta L_i^2 &= \Delta L_i^1 - \Delta L_{i-1}^1 \\ \Delta L_i^3 &= \Delta L_i^2 - \Delta L_{i-1}^2 \end{aligned} \tag{10}$$

where i denotes the observation epoch and ΔL_i^1, ΔL_i^2, ΔL_i^3 denote the first, second, and third differences. The accuracy is evaluated by calculating the mathematical expectation and variance of the third difference between the desired epochs. The mathematical expectation and variance are calculated as:

$$E(L) = \frac{1}{n}\sum_{i=1}^{n} \Delta L_i^3 \qquad \sigma_L^2 = \frac{1}{n-1}\sum_{i=1}^{n} [\Delta L_i^3 - E(L)]^2 \tag{11}$$

where n represents the number of observed epochs, $E(L)$ is the mathematical expectation, and σ_L^2 is the variance.

Taking the 2021 DOY 33 data from station WUH2 with a sampling rate of 1 s and no cycle skip after prior inspection, the carrier phase accuracy of each frequency band of BDS-3 and GPS was calculated. The results are presented in Tables 3 and 4.

Table 3 GPS carrier phase accuracy in each frequency band

system	GPS				
band	L1C	L1W	L2W	L2X	L5X
accuracy /mm	5.66	5.63	5.59	5.57	5.63

Table 4 BDS-3 carrier phase accuracy in each frequency band

system	GPS					
band	L1X	L2I	L5X	L6I	L7Z	L8X
accuracy /mm	7.89	8.14	8.13	8.19	8.3	8.29

The carrier phase accuracy of each band of BDS-3 is almost unchanged and fluctuates within a range of 0.5 mm. The largest carrier phase error of 8.3 mm appears in band B2b, and the smallest error of 7.89 mm occurs in band B1C. The carrier phase observation accuracy of BDS-3 is lower than that of GPS. The minimum error of GPS occurs in frequency band L2W, and is 2.3 mm smaller than that of BDS-3; the maximum error appears in frequency band L1C, and is 2.64 mm smaller than that of BDS-3. In the case of no cycle skip, the carrier phase positioning accuracy of BDS-3 in each frequency band exhibits little difference to that of GPS, and the difference is within 3 mm.

4.3 Performance Analysis for Relative Positioning

4.3.1 Dynamic shipborne experiment

In a real dynamic environment, the satellite signal is often out of lock or blocked. For the special constellation configuration of BDS-3, some high-latitude areas of China may suffer from frequently blocked signals from geostationary satellites because of their low elevation angle. Once the signal becomes occluded, the station will start to search for other satellites and solve the data again, which will increase the positioning error in this period. Therefore, it is necessary to conduct real-time positioning analysis using BDS-3 data through dynamic carrier experiments to study the dynamic positioning performance.

The first set of calculation examples use dynamic shipborne experimental data, collected on September 26, 2020, from 04:00:00-06:57:00 UTC. The observation environment of the whole measurement area is good, and there is basically no obstacle occlusion. As special hardware is required to receive BDS-3 satellite signals, the GAMG measurement station was selected as the reference receiver. This mobile station is located in the sea near Weihai City, China (37°35 '8.88 "N, 122°6' 41.67" E) and can receive most BDS-3 satellite signals. The distribution of the running track for this mobile station is shown in Figure 11, and the distribution of the onboard data installation instruments and equipment is shown in Figure 12: the receiver models on this dynamic station are Septentrio PolaRx5 and Trimble R9. The receiver had a sampling interval of 1 s and the baseline length was approximately 563 km. The LAMBDA method was used to fix the ambiguity.

In the actual dynamic environment, it is difficult to obtain the “true value” of the anchor point. Therefore, based on the principle of absolute distance between two antennas, the coordinate position of each antenna was calculated for every epoch, and then the distance between the two antennas was calculated as the evaluation standard[19].

Fig. 11 Trajectory diagram of shipboard

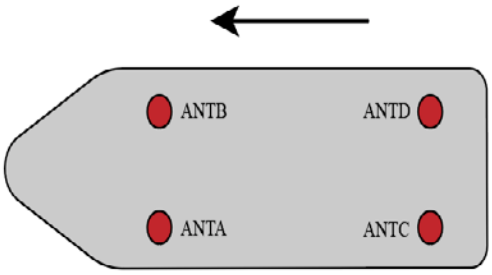

Fig. 12 Antenna position of experiment

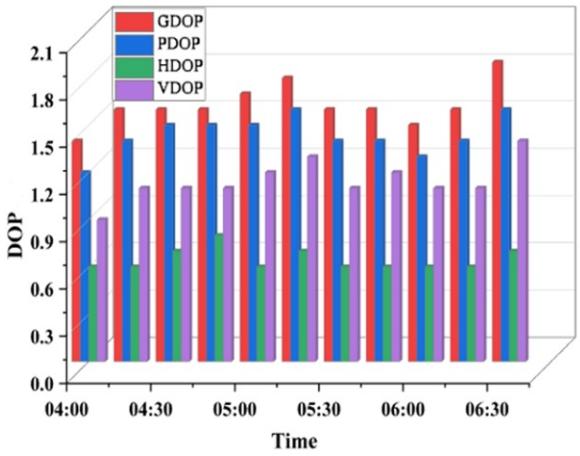

Fig. 13 Changes in satellite number and DOP

Figure 13 shows the changes in DOP values at antenna ANTA. The number of visible BDS-3 satellites ranged from 16-19. A higher number of satellites greatly improves the geometric structure of the observation satellites. From the DOP values in the figure, we find that PDOP and GDOP are higher than 1.8, HDOP is higher than 1.5, and VDOP is higher than 1.0.

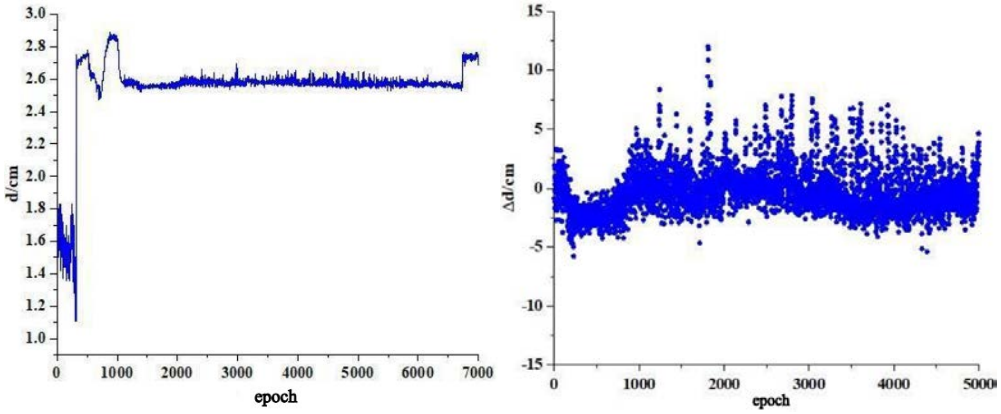

Fig. 14 ANTA-ANTD variations (left) and their differences from the true value (right)

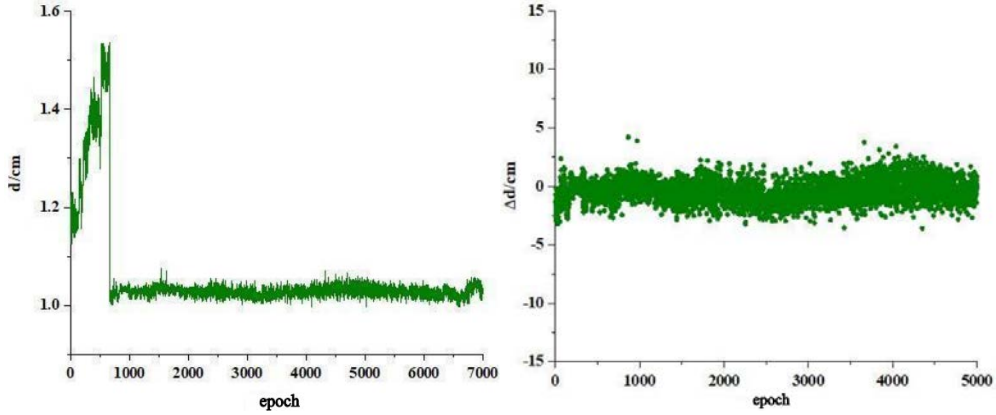

Fig. 15 ANTA-ANTB variations (left) and their difference from the true value (right)

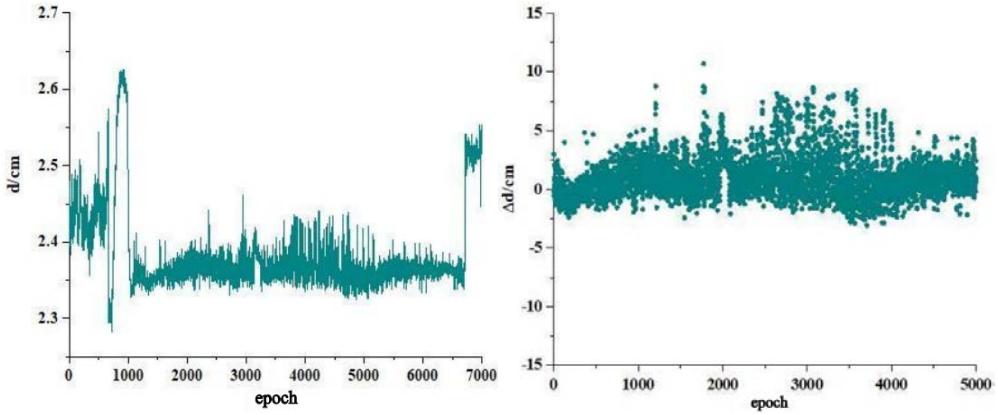

Fig. 16 ANTB-ANTD variations (left) and their difference from the true value (right)

Figures 14-16 (left) illustrate the fluctuations in the distance between antennas ANTA, ANTB, and ANTD over time. Under normal circumstances, the distance between them should be fixed. The right-hand panels in these figures represent the differences between the distance in each epoch and the true value (taken as the mean of multiple measurements). It can be seen from the diagram, three experiments of overall data calculating wave is small, only during the first half of the baseline weight appear larger deviation. Therefore, when using BDS-3 for real-time dynamic data positioning, the positioning accuracy between antennas is good after data convergence, basically fluctuating within a range of 5 cm.

Table 5 Shipboard data processing results

baseline	Min/cm	Max/cm	Mean/cm	Sdev/cm
ANTA-ANTD	-5.77	11.98	-0.28	1.89
ANTA-ANTB	-3.61	4.19	-0.41	0.94
ANTB-ANTD	-3.06	10.69	1.06	1.75

Table 5 presents statistics from processing the data of 5000 epochs after convergence. The largest deviation occurs between ANTA and ANTD, and the largest difference after convergence is 11.98 cm. The highest average value is for the distance between ANTB and ANTD. The mean distance between ANTA and ANTD and between ANTA and ANTB is less than 0.5 cm. In each case, the STD between any two antennas is less than 2 cm. Overall, the real-time dynamic positioning accuracy of BDS has reached the centimetre level, which is basically equivalent to the simulation experiment accuracy of static stations.

4.3.2 BDS-3 static experiment

To evaluate the difference in dynamic relative positioning performance between BDS-3 and GPS, a set of static data was dynamically processed using self-developed software. The true values for the experiment were taken from coordinates provided by ITRF. The specific parameters of the station are listed in Table 6.

Figure 17 shows that the real-time dynamic relative positioning of BDS-3 requires some time to locate the ambiguity. The positioning time is about 25 min. During this period, the data fluctuate significantly, while the ambiguity is fixed. The data fluctuations during the fixed ambiguity time are relatively small, and are related to the number of participating satellites. The dual-frequency GPS observations have an RMS of 6 mm, whereas those of BDS-3 have an RMS of 4–5 mm. This is related to the lack of BDS-3 satellite data observed during this period.

Table 6 Information of LEIJ-HUEG data

declaration	parameter
Antenna	LEIAR25.R4 LEIT
Receiver	JAVAD TRE_3
Time	2021-9-25 14:00:00-14:59:59
Sampling	1s
Baseline distance	520km
Elevation mask	10°
BDS-3 satellite	C24/C25/C26/C27/C33/C37/C38/C41/C42/C43/C46/C60

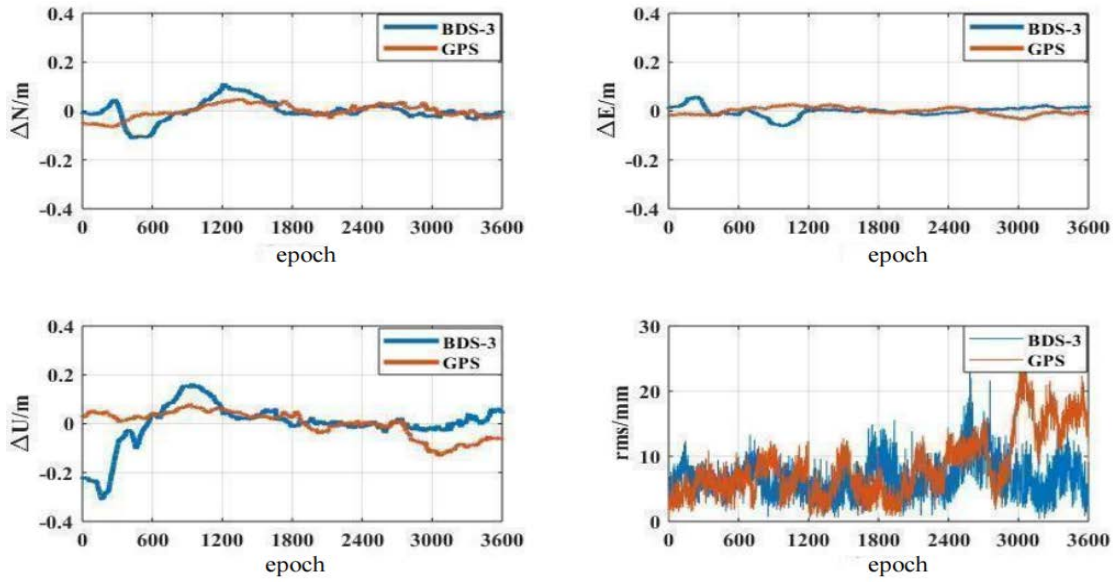

Fig. 17 Time series for the bias variation of position based on BDS-3/GPS

Table 7 Statistics of GPS/BDS-3 data processing results

System	Direction	Min/cm	Max/cm	Mean/cm	STD/cm
GPS	ΔN	-0.32	4.91	0.93	1.01
	ΔE	-0.36	2.58	-0.17	1.41
	ΔU	-13.21	6.02	-2.17	5.17
BDS-3	ΔN	-3.91	11.29	0.86	0.72
	ΔE	-1.93	2.47	0.33	2.24
	ΔU	-0.38	6.36	0.77	3.23

Table 7 summarizes the data of 2000 epochs after convergence. The largest deviation occurs in the vertical direction of GPS. In addition to the large deviation values, the real-time dynamic positioning accuracy of BDS-3 has reached the centimetre level. Once the ambiguity has been fixed, the data converge around 0, with horizontal fluctuations of 2-3 cm and vertical fluctuations of ~10 cm. The accuracy of real-time dynamic relative positioning after data convergence is basically equivalent to that of GPS.

5. Conclusions

(1) This study has analysed the complete BDS-3 data quality. The overall multipath error of BDS-3 is larger than that of GPS by around 5-10 cm. In terms of SNR, BDS-3 is basically consistent with each GPS station, and the average SNR basically fluctuates from 40-50 dB·Hz.

(2) In terms of service performance, in the case of no cycle skips, the carrier phase positioning accuracy of BDS-3 in each frequency band is similar to that of GPS, with the difference being within 3 mm. The four indices of DOP at most stations are lower than those of GPS. The maximum difference appears at station ULAB, where the GDOP of BDS-3 is 0.78 m lower than that of GPS. The double difference pseudorange residuals of each frequency band from the zero baseline range from 0.2-0.3 m, and the carrier phase residuals range from 0.17-0.48 cm. After data convergence, the relative positioning error fluctuates within 5 cm of the true value, although the fluctuations in the vertical direction are larger (within 10 cm).

(3) The quality indicators of existing BDS-3 signals were also evaluated. In terms of the pseudorange multipath error, the average value of the observation data at each station over 10 consecutive days was found to run in the order B1I>B2a>B2b>B3I>B2a+B2b>B1C. Frequency bands B2a+B2b and B2a have large SNRs, while the other bands have SNRs of 40-45 dB·Hz. The carrier phase accuracy of BDS-3 varies little in each frequency band, with fluctuations of only 0.5 mm.

Acknowledgements

This work is supported by the National Natural Science Foundation of China (42174021 and 42074028) and the Shandong Provincial Natural Science Foundation, China (ZR2021MD060).

References

[1] CSNO (China Satellite Navigation Ofce) (2018a) Development of the BeiDou navigation satellite system (version 3.0)

[2] CSNO (China Satellite Navigation Ofce) (2018b) BeiDou navigation satellite system open service performance standard (version 2.0)

[3] CSNO (China Satellite Navigation Ofce) (2019) BeiDou navigation satellite system signal in space interface control document open service signal B1I (version 3.0)

[4] Lu M, Li W, Yao Z, et al. (2019) Overview of BDS III new signals. Navigation - Journal of The Institute of Navigation, 66(4):19-35.

[5] Liu L, Zhang T, Zhou S, et al. (2019) Improved design of control segment in BDS-3. Navigation, 66(1):37-47.

[6] Yang Y, Gao W, Guo S, et al. (2019) Introduction to BeiDou-3 navigation satellite system. Navigation, 66(01): 7-18.

[7] Betz J W, Lu M, Morton Y, et al. (2019) Introduction to the special issue on the BeiDou navigation system. Annual of Navigation. 66 (1):3-5.

[8] CSNO (China Satellite Navigation Ofce) (2019) BeiDou navigation satellite system signal in space interface control document open service signal B2b (Beta version)

[9] Cai C, He C, Santerre R, et al. (2016) A Comparative Analysis of Measurement Noise and Multipath for Four Constellations: GPS, BeiDou, GLONASS and Galileo. Survey Review, 48(349): 287-295.

[10] Yang Y, Xu Y, Li J, et al. (2018) Progress and Performance Evaluation of BeiDou Global Navigation Satellite System: Data Analysis Based on BDS-3 Demonstration System. Science China Earth Sciences, 61(5): 614-624.

[11] Dai P, Ge Y, Qin W, et al. (2019) BDS-3 Time Group Delay and Its Effect on Standard Point Positioning. Remote Sensing, 11(15):1819-1848.

[12] Mu R, Dang Y, Xu C. (2020) BDS-3/GNSS Data Quality and Positioning Performance Analysis[C]. China Satellite Navigation Conference (CSNC) 2020 Proceedings: Volume I. Springer Singapore, Singapore, 368-379.

[13] Zhang Z, Li B, Nie L, et al. (2019) Initial assessment of BeiDou-3 global navigation satellite system: signal quality, RTK and PPP. GPS Solutions, 23(4):111-123.

[14] Zhu Y, Zheng K, Cui X, et al. (2021) Preliminary Analysis of the Quality and Positioning Performance of BDS-3 Global Interoperable Signal B1C&B2a. Advances in Space Research, 67(8): 2483-2490.
[15] Wu X, Zhou J, Wang G, et al. (2012) Multipath error detection and correction for GEO/IGSO satellites. Science China Physics, Mechanics and Astronomy, 55(7): 1297-1306.
[16] Bu J, Zuo X, Li X, Chang J, Zhang X. (2019) Evaluation and analysis on positioning performance of BDS/QZSS satellite navigation systems in Asian-Pacific region. Advances in Space Research, 63(7): 2189-2211.
[17] Teng Y, Wang J. (2016) A closed-form formula to calculate geometric dilution of precision (GDOP) for multi-GNSS constellations. GPS Solutions, 20(3): 331-339.
[18] Jian Z, Jaa C, Zwa C, et al. (2022) Signal quality and positioning performance of GPS/BDS-3/GLONASS/Galileo in polar regions. Advances in Space Research, 69(6): 2541-2554.
[19] Teunissen P. (1995) The least-square ambiguity decorrelation adjustment: a method for fast GPS ambiguity estimation. Journal of Geodesy, 70:65-82.
[20] He K (2015) GNSS kinematic position and velocity determination for airborne gravimetry. Technische Universität Berlin

Authors

Zhipeng Ding received his Master degree in Geodesy and Survey Engineering from China University of Petroleum (East China) in 2022. His research is focused on BDS-3 precise kinematic relative positioning.

Kaifei He is a professor at the China University of Petroleum (East China). He received his Ph.D. degree in Geodesy from the Technical University of Berlin (TU Berlin) in 2015 and studied in GFZ as a Ph.D. student from 2010 to 2014. Currently, his research focuses on GNSS navigation and positioning algorithms, underwater positioning, geodesy data processing, and software development.

Ming Li is a graduate student of China University of Petroleum (East China). His research focuses on BDS-3 high-precision real-time dynamic positioning.

Yu Wu is a graduate student of China University of Petroleum (East China). His research focuses on underwater navigation and positioning

Yue Zhang is a graduate student of China University of Petroleum (East China). His research focuses on retrieval of sea surface wind field from quad-polarization SAR.

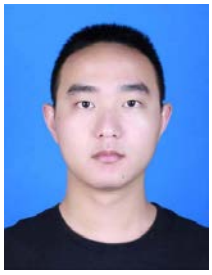

Jinquan Yang is a graduate student of China University of Petroleum (East China). His research focuses on the theory and method of GNSS/INS integrated navigation.